Na^+ imaging reveals little difference in action potential-evoked Na^+ influx between axon and soma

Ilya A. Fleidervish[1,3,4], Nechama Lasser–Ross[2,3], Michael J. Gutnick[1,3], William N. Ross[2,3]

[1] Koret School of Veterinary Medicine, The Hebrew University of Jerusalem, Rehovot, 76100, Israel

[2] Dept. of Physiology, New York Medical College, Valhalla, NY 10595, USA

[3] Marine Biological Laboratory, Woods Hole, MA 02543, USA

[4] Dept. of Physiology, Faculty of Health Sciences, Ben–Gurion University of the Negev, Beer Sheva 84105, Israel

Address for correspondence:

Ilya A. Fleidervish,
Department of Physiology,
Faculty of Health Sciences, POB 653,
Ben Gurion University
Beer–Sheva 84105, Israel
Tel: 972–8–6477307
FAX: 972–8–6477628
email: ilya.fleidervish@gmail.com

Figures: 8

Pages: 26

Supplementary Figures: 5

Supplementary Movies: 3

Abstract

In cortical pyramidal neurons, the axon initial segment (AIS) plays a pivotal role in synaptic integration. It has been asserted that this property reflects a high density of Na^+ channels in AIS. However, we here report that AP–associated Na^+ flux, as measured by high–speed fluorescence Na^+ imaging, is about 3 times larger in the rat AIS than in the soma. Spike evoked Na^+ flux in the AIS and the first node of Ranvier is about the same, and in the basal dendrites it is about 8 times lower. At near threshold voltages persistent Na^+ conductance is almost entirely axonal. Finally, we report that on a time scale of seconds, passive diffusion and not pumping is responsible for maintaining transmembrane Na^+ gradients in thin axons during high frequency AP firing. In computer simulations, these data were consistent with the known features of AP generation in these neurons.

Introduction

In neocortical pyramidal cells, as in many CNS neurons, the axon initial segment (AIS) plays a pivotal integrative role because it has a lower threshold for action potential (AP) generation than the soma and dendrites[1], and thus controls both the transformation of dendrosomatic synaptic input into spike output, and the backpropagation of APs into the dendrites. Properties of Na^+ channels in the AIS are reported to differ from those in other regions of the cell. For example, several authors have reported that the activation voltage of Na^+ channels is 6–14 mV more hyperpolarized in the axon than in the soma[2–4]. Moreover, the AIS has been implicated as the primary source of persistent Na^+ current (I_{NaP})[5, 6].

One major subject of disagreement is whether the density of Na^+ channels is significantly greater in the AIS than in the soma. An early computational study[7] reported that in an anatomically correct compartmental model of a pyramidal neuron with identical Na^+ channel properties in all regions, Na^+ channel density in the AIS must be orders of magnitude higher in the AIS than in the soma to simulate the lower axonal threshold. However, subsequent patch recordings from the AIS suggested that the density in the two regions is similar[2, 3, 8]. More recently, in the same paper in which patch recordings indicated equal densities, the authors[3] presented several arguments why this result might not be correct, and asserted that the true Na^+ channel density in the AIS is much higher than in the soma or dendrites. A similar conclusion was reached based on recordings from blebs that form when cortical axons are cut[4].

In the present study, we used high–speed fluorescence imaging of the Na^+ indicator SBFI[9, 10] to quantitatively describe the Na^+ dynamics that accompany subthreshold depolarizations and single and multiple AP generation in axons, dendrites and somata of layer 5 neocortical neurons. Our measurements of Na^+ flux in axon, soma and basal dendrites suggest that the ratios of Na^+ channel densities in these regions is approximately 3:1:0.3. They also provide evidence for the axonal location of the subthreshold persistent Na^+ conductance and show that diffusion is the main removal mechanism following Na^+ entry in the AIS and first node of Ranvier.

Results

Na^+ transients in the axon decay faster than in the soma

In 197 layer 5 pyramidal neurons, changes in SBFI fluorescence during single or multiple APs elicited by brief somatic current injections were recorded in the soma and nearby axon and basal dendrites. All the fluorescence transients were blocked by bath–applied tetrodotoxin (TTX; 1 μM; n=4). During experiments, axons were distinguished from the other fine processes because they emerged from the soma opposite the apical dendrite and had distinctive Na^+ transients (see below). Thirty six neurons were examined live in a two–photon microscope after the physiological experiment. In these cells, axons were readily distinguished from basal dendrites by their lack of spines (**Fig. 1a**), confirming the determination that had been made

during recording. These reconstructions were used to measure the dimensions of the axon, soma, and dendrites, which were later used to estimate the relative Na^+ fluxes in the different compartments.

Figure 1b shows the Na^+ transients elicited by a single AP and a train of 10 APs in a representative neuron. Averaged Na^+ transients (n=20) elicited by single APs were prominent only in the axons, and were poorly or not at all detectable in soma and dendrites (see also **Supplementary Movie 1**). The greatest change in axonal SBFI fluorescence occurred 10–30 μm from the soma. $[Na^+]_i$ grew rapidly (10–90% rise time less than 10 ms), and decayed rapidly with a time constant of 200–600 ms. At distances beyond 35–50 μm, in the presumed myelinated region of the axon [11], Na^+ transient amplitudes were smaller and their peaks were progressively delayed (**Fig. 1b**). The amplitudes and time courses of the fluorescence transients are expected to accurately reflect the entry and removal of Na^+ from the cell since Na^+ is not significantly buffered either by components of the cytoplasm or by the Na^+ indicator (see Methods).

When trains of 3 or more APs were generated, Na^+ signals were also detected in the soma and basal and apical dendrites, although they remained largest in the proximal axon (**Fig. 1b**). The most dramatic difference was in the rates of Na^+ clearance. In the soma and dendrites $[Na^+]_i$ either stayed at a plateau level or decayed slowly after the end of the spike train; $[Na^+]_i$ recovery was often not complete even 10 s following the cessation of stimuli. In the proximal axon, by contrast, $[Na^+]_i$ rapidly declined immediately upon termination of the stimuli.

Rapid Na^+ removal in axons is not due to active transport

We used 2 experimental manipulations to decrease the activity of the pump. First, we cooled the slices from 33°C to 23°C. This had only minimal effect on the decay time constant of the Na^+ transients in the proximal axon (τ =0.42 ±0.16 s at 33°C vs. 0.54 ±0.10 s at 23°C, $p>0.05$, n=4, **Fig. 2**). Second, bath–applied oubain (100 μM), which blocks the Na^+/K^+–ATPase [12], had little or no effect on axonal Na^+ clearance (τ=0.34 ±0.18 s in control vs. 0.37 ±0.21 s with oubain, $p>0.05$, n=3). Therefore, in the time frame of our experiments, active transport is not responsible for the dynamics of Na^+ clearance from the axons.

Na^+ dynamics reflects localized Na^+ influx and diffusion

We next examined whether spike evoked Na^+ entry and subsequent axial diffusion is sufficient to account for the time course and observed rapid Na^+ clearance in the axons by comparing experimentally observed Na^+ transients with results of numerical simulations. We built a simplified compartmental model that encompassed the fundamental morphological features of a layer 5 pyramidal neuron. In the model, the first 35–50 μm of the axonal length were assumed to be uncovered by the myelin sheath [11] and to possess a uniform Na^+ channel density ~3 times higher than that of the soma (see Methods). The subsequent, myelinated

segment possessed no Na^+ channels. In addition to Hodgkin–Huxley type Na^+ and K^+ conductances, the model incorporated longitudinal diffusion of Na^+ ions between neighboring compartments with a diffusion coefficient of 0.6 $\mu m^2/ms$ (reference 13); no mechanism for Na^+ extrusion was included. Thus, the spatio–temporal patterns of the simulated $[Na^+]_i$ transients solely reflected transmembrane influx into the 'active' compartments which possess Na^+ channels (soma, AIS), and Na^+ diffusion into compartments, which either possess no Na^+ channels (myelinated segments) or are large sinks because they have a relatively small surface to volume ratio (soma). In all active locations in the model, $[Na^+]_i$ grew throughout the AP train; it continued to grow after the termination of the train in the passive myelinated internodes, reflecting diffusion of Na^+ from the adjacent AIS (**Fig. 3b, c**). The initial parts of the decay time constants of the simulated Na^+ transients were fastest at the most distal and proximal extremes of the AIS, and increased towards its center. Within several tens of milliseconds, however, the rate of Na^+ diffusion from the AIS into the myelinated internodes slowed, reflecting the progressive decrease in the steepness of the Na^+ concentration gradient. By contrast, the steep axo–somatic Na^+ gradient persisted, because $[Na^+]_i$ in the relatively immense soma remained low and nearly constant.

The model closely mimicked experimentally observed changes in fluorescence during a single AP (**Fig. 3a**) as well as AP trains (**Fig. 3b, c**). Amplitudes of $[Na^+]_i$ elevations were largest in the AIS, where time–to–peak was fastest and uniform throughout the segment (**Fig. 3a, b**). In the first myelinated segment, where simulated Na^+ transients only reflected longitudinal Na^+ diffusion from the AIS, time–to–peak grew and amplitude declined as a function of the distance from the site of Na^+ influx (**Fig. 3a, b, d**).

Finally, we compared the Na^+ transients in cortical neurons to those in cerebellar Purkinje cells (**Supplementary Fig. 1**), which possess a much shorter AIS of only 15 μm (reference 14). Both the spatial distribution of times–to–peak of the Na^+ transients along the axonal length and the half–width at a distance of 10 μm from the hillock differed significantly between the two types of neurons (**Fig. 3e**). The difference was completely predicted by diffusion models by changing the AIS length of 38 μm in cortical neurons to 15 μm for Purkinje cells (solid traces in **Fig. 3e**).

Relative AP–evoked Na^+ influx in different compartments

Because the dynamics of the Na^+ transients for short times can be entirely described in terms of influx and diffusion, we can use the fluorescence measurements to estimate the relative fluxes of Na^+ ions into the different compartments during AP generation. However, inference of spike–evoked Na^+ influx per unit membrane area (Q_{Na}) from the imaging data requires careful consideration of differences in surface to volume ratio, background tissue fluorescence and other technical factors. We used three different approaches to evaluate relative Q_{Na}.

Our first approach focused on the shapes of the Na^+ transients in the AIS, the soma, and the basal dendrites. **Figure 4a** shows Na^+ transients elicited by trains of 10 and 100 APs in a representative neuron. Under both protocols $[Na^+]_i$ grew steadily throughout the train in all neuronal compartments. In the AIS, $[Na^+]_i$ declined rapidly after reaching its peak, achieving a steady level in about 2 seconds. In the soma and basal dendrites the $[Na^+]_i$ also stopped rising at the end of the train, but did not fall significantly over the next few seconds. The steady level in all three compartments was about the same, indicating that diffusional equilibrium was achieved.

The rapid recovery of the AIS signal shows that the peak $[Na^+]_i$ change in that compartment was much higher than the end–of–train $[Na^+]_i$ in the soma. But it is not immediately clear if this results from a higher Q_{Na} across the membrane or because the axon is thinner than the soma. That the dendritic signal did not decline after the train indicates that the $[Na^+]_i$ change in the dendrite was close to the $[Na^+]_i$ change in the soma. Since the surface–to–volume ratio of the dendrite is much greater than that of the soma, this closeness suggests that Q_{Na} into the basal dendrite must be less than Q_{Na} into the soma.

To obtain a more quantitative estimate of the Q_{Na} ratio among the three compartments, we measured the peak and steady state $\Delta F/F$ values and then constructed a simple compartmental model to reproduce these values. The $\Delta F/F$ steady–state to end–of–train ratio of the AIS Na^+ transients was 0.22±0.07 (mean ± SD; n=7) following a train of 10 APs and 0.47±0.08 following a train of 100 APs; in the basal dendrites the ratios were 1.29±0.22 and 0.92±0.13, respectively.

We next performed computer simulations to find the ratio of channel densities consistent with the measured $\Delta F/F$ time courses and relative magnitudes. The somatic Na^+ channel density was kept constant, while Na^+ channel density in the process (either axon, consisting of a 40 μm long AIS followed by a myelinated internode, or basal dendrite) was systematically varied. **Figure 4b** shows that in order to match the experimentally determined steady–state to end–of–train $\Delta F/F$ ratios, the Na^+ channel density in the AIS has to be 1–3 times the somatic density and the Na^+ channel density in the basal dendrite has to be 0.1–0.3 times the somatic density. The presence of a myelinated segment made only a small difference in the predicted recovery curves (not shown).

A second approach to estimating relative Q_{Na} from the imaging data relies on the following considerations:

(1) $\Delta[Na^+]_i \sim \frac{\Delta F}{F}$, where $\Delta[Na^+]_i$ is the Na^+ concentration change per spike and $\frac{\Delta F}{F}$ is the fractional change in SBFI fluorescence. This relationship holds if the change in fluorescence is linear, which should be true since the K_D for the Na^+–SBFI interaction is high (26 mM [15]) and $\Delta F/F$ values are « 1.

(2) $\Delta[Na^+]_i = \frac{Q_{Na}}{V}$, where Q_{Na} is the transmembrane Na^+ influx per spike and V is the volume of the region of interest, assuming the removal rate of Na^+ is slow compared to the rate

of entry. Assuming that the indicator concentration is uniform throughout all compartments, which is reasonable for the peri–somatic region after 15 min of dialysis, then V ~ F and:

(3) $Q_{Na} \sim \Delta F$

since the fluorescence of SBFI in a region should be proportional to the volume of the region. This relationship allows us to directly compare the charge entries in different regions. Additional technical considerations are described in **Methods**.

We measured ΔF in the soma, AIS, and basal dendrites following trains of 5 APs at 10 ms intervals (**Fig. 5a**) or 10 APs at 30 ms intervals. We found that $\Delta F_{AIS}/\Delta F_{soma} = 2.05\pm0.27$ for the faster train (mean±SD; n=11) and 1.54±0.42 for the slower train (n=19), measured within a region around the soma and a rectangle over the axon. The ratios were sensitive to changes in the areas of the circles or rectangles (**Supplementary Fig. 2b**) but the resulting error was not greater than 20%. If we correct the amplitude determined from the slower train for the reduction due to axial diffusion (increase by ~40%) then that ratio becomes 2.16±0.59, which is close to the ratio determined from the faster train. The average is 2.10±0.43. Applying an additional correction factor of 0.78 for the difference in surface/cross section for the axon and soma (see **Methods)** we estimate that ratio of Q_{Na} in the two compartments, $Q_{AIS}/Q_{soma} = 2.69\pm0.55$.

We made a similar comparison between the axon and basal dendrites (**Fig. 5a**). We found that $\Delta F_{axon}/\Delta F_{basal} = 8.64\pm0.86$ for spikes at 10 ms intervals (mean±SD; n=11) and 6.01±2.69 for spikes at 30 ms intervals (n=9). We still had to apply a correction for diffusion for the slower train, but there was no need to correct for differences in surface/cross section since both compartments were assumed to be cylinders. After correcting and averaging we found $Q_{AIS}/\Delta Q_{basal} = 8.4\pm3.6$.

The third approach for estimating Q_{Na} starts from the same equations. Since there is almost no buffering of entering Na^+ ions (see Methods):

(4) $Q_{Na} = k \cdot C_{Faraday} \cdot \frac{\Delta F}{F} \cdot \frac{volume}{surface\ \ area}$, where *k* is the change in $[Na^+]_i$ that causes ΔF/F=1% , $C_{Faraday}$ is Faraday's constant, ΔF is the AP–evoked change in fluorescence, F is the resting fluorescence of SBFI in the volume (equal to the total measured fluorescence minus F_a, the tissue autofluorescence). Typically, the autofluorescence F_a was about 5% of F in the soma and 35% of F in the axon and basal dendrites. The ratio of volume–to–surface area was assumed to be diameter/6 for a quasispherical soma and diameter/4 for the cylindrical AIS and basal dendrites. The diameters of the soma, axon, and basal dendrites for each neuron were estimated from 2–photon reconstructions.

Figure 5b shows $\frac{\Delta F}{F}\frac{volume}{surface\ area}$ (which is proportional to Q_{Na}) in each compartment. In the soma, AIS, and basal dendrites the mean values of $\frac{\Delta F}{F}\frac{volume}{surface\ area}$ were

0.30±0.06 (n=14), 0.78±0.14 (n=14) and 0.08±0.01 % μm (n=9), respectively. Q_{Na} in soma, AIS and in basal dendrites, assuming k=0.4 mM per 1% ΔF/F (reference[15]) was 11.8±2.1, 30.1±5.7 and 3.3±0.5 fC/μm^2, respectively. Using these numbers we found that Q_{AIS}/Q_{soma}=2.95±0.45 (n=14) and Q_{AIS}/Q_{basal}=8.88±1.74 (n=9), close to the estimates obtained by the first two approaches (**Fig. 5c**).

In these experiments, the $[Na^+]_i$ changes were elicited by trains of APs. We also evaluated the SBFI fluorescence changes associated with single APs, although the small signal size and the inability to completely eliminate vibrations made the analysis more difficult. In two neurons in which the single spike changes could be clearly measured in both the soma and the axon, the Q_{AIS}/Q_{soma} ratio for one AP was similar to that determined with spike trains (**Supplementary Fig. 3**). Because the rise time of the single spike signals was much faster than the fall time there was no need to correct for diffusion.

Sodium dynamics at nodes of Ranvier

In 8 cortical neurons nodes were identified by the characteristics of their Na^+ transients (see below). In 4 of these neurons, subsequent 2–photon reconstructions revealed thin collateral axonal braches which originated from the axonal trunk at the presumed node location (**Fig. 6a**). An additional node was found in the axon of a cerebellar Purkinje cell (not shown). In both cell types, the first nodes were found within 95–115 μm from the soma. In the two axons in which second nodes of Ranvier were identified (both in Na^+ imaging experiments and in 2–photon reconstructions), they were located 22 and 28 μm from the first node.

Physiologically, nodes were identified as isolated locations where the time course of the Na^+ transient was in synchrony with the spike train (**Fig. 6a**). When these Na^+ elevations occurred, they were evident for distances of 10–20 μm along the axonal length, obviously longer than the dimensions of a central node of Ranvier[16]. The maximal amplitudes of nodal Na^+ transients elicited by 5 APs at 10 ms intervals (ΔF/F =0.5 to 2%) were <10% of those in the AIS of the same neuron (**Fig. 6a**). The amplitude was maximal in the center of a segment and decayed in both directions (**Fig. 6a, c, Supplementary Fig. 4**).

Because the nodes are small, Na^+ ions diffuse laterally almost as quickly as they enter across the nodal membrane. Computer simulations show that diffusion–mediated $[Na^+]_i$ equilibration between the nodal and internodal volumes should be nearly complete within milliseconds (**Fig. 6b**), and that within 10 ms after the peak of the AP, more than 90% of Na^+ ions that enter a 1 μm long node are already in the internodal region. By contrast, 10 ms after an AP in the 48 μm long AIS, dissipation of the Na^+ gradient is minimal.

We cannot measure the peak $[Na^+]_i$ in the node even if we record the fluorescence change at 500 frames/s, because Na^+ ions diffuse away from the node too quickly. However, since diffusion is the primary clearance mechanism, we expect that all of the Na^+ that entered at the node will be contained, for a short while, within a region extending 20 μm to either side. Thus,

integration of the $[Na^+]_i$ change over this region 10 ms after the spike train, estimates the total charge transfer via nodal Na^+ channels. This measure was similar to the charge transfer density in the AIS (**Fig. 6c**).

This conclusion was supported by computer simulations where the AIS Na^+ channel density was held constant, while Na^+ channel density in the first node was varied (**Fig. 6c**). Comparison of the experimentally determined ΔF/F changes in this cell to those predicted by the model indicates a nodal Na^+ channel density of the same order of magnitude as in the AIS (**Supplementary Fig. 4**).

$[Na^+]_i$ changes associated with persistent Na^+ conductance

To examine $[Na^+]_i$ changes due to activation of I_{NaP} we applied subthreshold pulses of varying durations. These depolarizations evoked a significant change in SBFI fluorescence in the axon that persisted throughout the pulse and were completely and reversibly blocked by TTX (not shown, n=3), indicating that they reflected Na^+ influx through voltage–sensitive Na^+ channels. The traces in **Figure 7a** are representative of all 43 cells studied with this protocol. In all neurons, the amplitude of the axonal Na^+ transients elicited by 1 s subthreshold depolarizations was comparable to or larger than the transients elicited by single action potentials, even though the signal associated with the prolonged subthreshold pulse must have included significant Na^+ diffusion out of the AIS. Even with subthreshold depolarizations as long as 3 s, the signal was maintained throughout the duration of the pulse, indicating the truly persistent nature of the underlying Na^+ current (**Fig. 7b**). I_{NaP} undergoes some slow inactivation [17], but this was not evident in the imaging data.

In most experiments, there was no detectable persistent Na^+ entry in the adjacent basal dendrite (**Fig. 7a**) and soma (**Fig. 7c**) following subthreshold depolarization. Thus, extensive signal averaging revealed a small somatic signal in only 3 of the 12 cells. **Fig. 7c** shows that the AIS:soma ratio of the amplitudes of the signal evoked by a 1 s subthreshold depolarization was much larger than the ratio of amplitudes evoked by a train of 10 APs. This result was found even though Na^+ diffusion out of the AIS should have a much greater effect on peak axonal ΔF/F during the prolonged pulse than on the rapid, spike–evoked signal.

To evaluate the contribution of I_{NaP} at suprathreshold potentials, we examined the Na^+ transients generated during ramps under voltage clamp. Slow voltage ramps from –70 mV to –40 mV or to 0 mV (**Fig. 7d, e**) were applied to somata with K^+ currents blocked by Cs^+ as the main intracellular cation, and Ca^{2+} currents blocked by adding 200 μM Cd^{2+} to the bath [6, 18]. Analysis of ramp–induced Na^+ transients in 21 neurons showed that voltage onset of I_{NaP} generation (–57 ± 5 mV) was accompanied by a parallel onset of the change in AIS SBFI fluorescence (–57 ± 6 mV), while somatic and basal dendritic Na^+ signals were first detected at more depolarized potentials (–41 ± 6 mV). The signals in the soma and dendrites correspond primarily to Na^+ entry into those regions and not diffusion from the axon, because the signals began to decline as

soon as the ramp ended. This difference in onset voltages suggests that I_{NaP} has shifted voltage dependence in the axon compared to the other compartments.

Implications of Na^+ flux distribution for AP generation

In axonal recordings APs maximal rates-of-rise are greater than 1000 V/s (reference 3) and the preferred location for spike initiation is near the distal end of the AIS[11, 19]. Some studies[3, 7] suggest that a high axon:soma ratio of Na^+ conductances is required to account for these observations. Since our imaging experiments found that the conductance ratio between these compartments is not high, we wanted to see if a model with a reasonable set of parameters could be constructed that would match our observations and still produce APs with these characteristics. We found that we could simulate the fast upstroke despite the much lower AIS Na^+ channel density by assigning faster, more realistic values to the kinetic parameters of the Na^+ channels (**Fig. 8a**).

The velocity of the action potential upstroke is given by: $dV/dt = I_{Na}/C_{local}$, where I_{Na} is the current flowing through the Na^+ channels and C_{local} is the membrane capacitance (assuming that I_{Na} is significantly larger than other currents). Thus, the smallest I_{Na} that could underlie a dV/dt of 1000 V/s is ~10 pA/μm^2 (assuming C=1 μF/cm^2), which corresponds to a g_{Na} of 200 pS/μm^2 (assuming that at the point where dV/dt is maximal the driving force for Na^+ is 50 mV). This is the value if Na^+ channel activation is instantaneous; it will be larger if the time constant of Na^+ channel activation (τ_m in the Hodgkin–Huxley formalism) is slow. The value of τ_m at physiological temperature is not known and is difficult to measure. Generally, the bandwidth used for Na^+ channel recordings in CNS neurons is 2 kHz (–3dB, 8–pole Bessel filter) (e.g. references [2, 3]), which optimizes the signal to noise ratio and permits accurate capacitive transient subtraction. However, as can be seen in **Figure 8a** (top), recording at 2 kHz at 23°C distorts and slows the onset kinetics of currents if τ_m is faster than about 120 μs.

The most accurate estimate of Na^+ channel activation kinetics in central neurons was made from mossy fiber boutons[20]. Recording at 23°C, with a 10 kHz low–pass filter, the authors reported τ_m of 38 μs and 14 μs for 0 mV and +40 mV, respectively. At 32°C, if Q_{10}=3 and the rate is nonsaturating, τ_m will be13 μs and 5 μs, respectively. The lower panel of **Figure 8a** shows that when τ_m is in this range very fast action potentials are possible with considerably lower current density. The APs are shown at the distal end of the AIS, where they are most isolated from the soma by the thin AIS.

We examined in simulations the effects of density and properties of the Na^+ channels in the AIS at the site of AP initiation (**Fig. 8b**). In all models, voltage–dependence of axonal gNa was shifted by – 6 mV compared with somatodendritic channels [2–4, 21]. When Na^+ conductance was equal in the soma and AIS (250 pS/μm^2), somatic current injection (2 ms, 1 nA) produced a relatively slow and uniform regenerative response across soma, proximal axon and dendrites (**Fig. 8b**, top, left; see also **Supplementary Movie 2**). A three–fold increase in the AIS

conductance, however, was sufficient to change this pattern towards axonal spike initiation (**Fig. 8b**, top, right). The AP voltage threshold was shifted to more negative potentials and axo–somatic delays and voltage gradients were greater in models with a faster τ_m (τ_mx0.2, **Fig. 8b**, bottom, left) and the axosomatic difference was even more evident when persistent Na^+ conductance was added to the AIS (**Fig. 8b**, bottom, right; see also **Supplementary Movie 3**). In all these models APs backpropagated over the dendrites following initiation in the AIS.

Discussion

Na^+ imaging allows us to quantitatively evaluate the characteristics and density of sodium channels in thin neuronal processes, providing a complementary approach to electrophysiological and immunocytochemical techniques, which have sometimes been controversial. For example, immunocytochemical measurements[3] might over–estimate channel density by labeling channel proteins that are not functional and therefore may not be relevant to excitability. The main conclusions from our study are: 1) Na^+ channel density (or more precisely, Na^+ current density per AP) in the soma is about 3 times lower than in the AIS and 3 times greater than in basal dendrites. 2) In nodes of Ranvier, AP–induced Na^+ influx is of the same order of magnitude as in the AIS. 3) At functionally critical subthreshold range of voltages, I_{NaP} is primarily generated by the AIS. 4) Passive diffusion, not active pumping, is responsible for rapid clearance of Na^+ from beneath the membrane of the AIS and node of Ranvier during repetitive AP generation.

Na^+ channel density in different neuronal compartments

The finding that AP–induced Na^+ flux density is about 3 times greater in the AIS than in the soma would indicate the same ratio of channel densities if the amplitude and shape of the AP and the temporal kinetics of the channels were the same in the two regions. In the proximal AIS, the maximal rate of rise of the AP is about twice that of the somatic AP, while spike amplitudes are similar in both compartments[3]. Because the time to peak is about 20–30% briefer than in the soma, we would underestimate the ratio of peak gNas by about that amount if we use the axon:soma flux ratio we measured to estimate the conductances. On the other hand, the Na^+ current is entirely inactivated by the time of the peak of the AP in the isolated pyramidal cell soma[22]. Because the peak is reached earlier in the axon, there may be some Na^+ current during repolarization. Since this is an additional current going through the same channels that are open on the rising phase, the axon:soma flux ratio of 3:1 that we record probably reflects an even smaller ratio of peak gNas, and hence, channel densities. In fact, several groups[2,3,8] estimated channel densities based on electrophysiological recordings from cell attached or excised patches in the AIS and arrived at estimates in the AIS that are less than 3 fold higher than their estimates for the soma.

One suggestion[3] is that the ratios determined from patch recordings do not reflect the effective physiological channel density because Na^+ channels in the AIS are anchored to the

cytoskeleton and do not completely reveal themselves in patch recordings. This analysis is based on experiments which disrupted the connection of Na^+ channels to ankyrin G and thereby increased the apparent channel density. However, even if that interpretation is correct, there was only a three fold increase in density, which is still closer to the range of cell-attached measurements and our determination than to the factor of ~40–50 proposed based on other considerations[3].

The relative AP– evoked $[Na^+]_i$ changes we recorded in different regions were qualitatively similar to those reported in pyramidal neurons[3] and in other cell types[23,24]. All experiments agree that the fractional fluorescence change ($\Delta F/F$) following a depolarizing stimulus is much lower in the soma than in the AIS. However, $\Delta F/F$ reflects concentration change and not Q_{Na}, which is the parameter closest to channel density. When we used ΔF, which is more closely related to current density, the fluorescence changes in the two compartments were similar. In our other approach, where we compared $[Na^+]_i$ changes, but corrected for the difference in surface/volume, we came to the same conclusion.

Another experimental observation that suggested[3] a high density of channels in the AIS is the extremely fast rise time of the action potential in AIS. The model used in that analysis[3] probably required a high channel density in order to compensate for a high estimate of the Na^+ channel activation time constant, τ_m. We were able to simulate the same fast rise time with a much lower Na^+ conductance in the AIS, provided we assigned faster values (based on other experiments[20, 25]) to the kinetic parameters of the Na^+ channels (**Fig. 8**). Another argument[3] for a high Na^+ channel density in the AIS is that it is required to support the experimental finding that action potentials initiate at the distal portion of the AIS and not in the first node of Ranvier. This argument, however, depends critically on the relative Na^+ channel density in the nodes and in the AIS. The model referred to in that argument[3] used estimated values based on recordings in rat peripheral nerve[20] (21,000 channels per node). Our evidence (**Fig. 6**) indicates that in the axon of the pyramidal neuron, where nodes are smaller and closer together, the current density is smaller. There is no need, therefore, to postulate high Na^+ channel density in the AIS.

Our findings about the relative basal dendrite/axon current densities are consistent with previously reported imaging data[3] As with the axonal data, the interpretation of these results in terms of channel densities depends on the relative spike amplitudes in the different compartments. There is still some disagreement about AP properties in the basal dendrites. Direct patch recordings from the basal dendrites suggest attenuated back–propagation of APs[26], while experiments using voltage sensitive dyes found less attenuation[27]. If the spikes are attenuated, we would expect a slightly higher relative channel density than the estimate from Q_{Na}. Since our measurements were made less than 30 μm from the soma, where attenuation is minimal, we expect the correction to be small.

Persistent Na^+ current

Our imaging data confirm that in the functionally critical subthreshold voltage range persistent Na^+ conductance in Layer 5 pyramidal cells is generated predominately in the axon as previously reported[6] The voltage clamp experiments indicate that at more depolarized potentials, persistent Na^+ conductance is also activated in the somatic and dendritic membranes. It remains unclear whether different voltage dependence of the persistent conductance in these compartments parallels the reported difference in voltage dependence for the transient Na^+ current[2–4, 21]. It is generally accepted that the activation voltage of I_{NaP} is more negative than that of the transient current, although the extent of the leftward shift is not known (for review, see 28). Thus, the axonal I_{NaP} undoubtedly contributes to the lower threshold of the AIS [1, 8].

Diffusion and clearance of Na^+ ions

Many types of central neurons fire high–frequency bursts that propagate via myelinated axons to target cells with a timing precision that is critical both for ongoing communication between neurons[29] and for synaptic plasticity [30]. The structural relationships between the axonal membrane and the myelin sheath are optimized for initiation and rapid, saltatory propagation of APs. Our results suggest an additional function for this organization: the geometrical dimensions of myelinated and non–myelinated segments of the axon permit rapid, energy efficient restoration of transmembrane Na^+ gradients beneath the excitable membrane. We showed both experimentally and using numerical simulations that in myelinated axons, APs are associated with a striking heterogeneity in $[Na^+]_i$ over a short length of AIS–soma and node–internode assemblies. (We did find small voltage dependent Na^+ and Ca^{2+} entry in the myelinated region (**Supplementary Fig. 5**), consistent with previous observations[31, 32], but the spike evoked Na^+ entry in this region was much smaller than in the AIS or first node). The resultant sharp Na^+ gradients facilitate rapid recovery of $[Na^+]_i$ by diffusion. Of course, Na^+ ions which enter the axoplasm during activity will eventually have to be extruded by the Na^+,K^+ – ATPase, which uses about a half of the brain energy budget for this purpose[33]. However, in the time frame of milliseconds, it is Na^+ clearance mediated by lateral diffusion which prevents Na^+ accumulation in the functionally critical, non–myelinated segments. Moreover, while Na^+ influx is predominately restricted to the initial segment and to the periodic nodes of Ranvier, the Na^+ extrusion mechanism utilizes the whole neuronal membrane, including myelinated internodes and soma where the pump is present[34].

Acknowledgements

We thank Satoshi Manita for excellent help with the preparation of slices. Supported by US–Israel BSF Grant (2003082), Grass Faculty Grant from the MBL, NIH Grant (NS16295), Multiple Sclerosis Society Grant (PP1367), and a fellowship from the Gruss Lipper Foundation.

Author contributions

I.A.F., N.L.R., M.J.G. and W.N.R. designed the study, performed the cortical experiments and co–wrote the paper. N.L.R. and W.N.R. performed the cerebellar experiments. I.A.F. constructed the computational models.

Figure Legends

Figure 1 Time course of AP induced $[Na^+]_i$ changes is different in different compartments.

(a) Reconstruction of 58 optical sections taken at 1 μm intervals through part of a layer 5 pyramidal neuron filled with 2 mM SBFI.

(b) *Left*, The same neuron as seen during the fluorescence imaging experiment with NeuroCCD–SMQ camera. The rectangles and arrows indicate the regions from where fluorescence measurements were obtained. *Middle*, Averaged Na^+ transients (n=20) elicited by a single AP were only prominent in the axon. Between 0–30 μm the transients peaked sharply at the time of the spike, while between 30–40 μm the rise was more gradual. *Right*, Averaged Na^+ transients (n=10) elicited by train of ten spikes (33 Hz) were detected in soma, basal and apical dendrites, although they were larger in the axon. In the proximal axon $[Na^+]_i$ grew throughout the duration of the train; immediately upon the train end, the $[Na^+]_i$ declined rapidly. In soma and dendrites $[Na^+]_i$ stayed at nearly steady level after the end of the spike train.

Figure 2 Active transport cannot account for the rapid Na^+ clearance in the axon.

Left, the decay of axonal Na^+ transients ~20 μm from the soma elicited by a train of 10 action potentials was not significantly affected by heating of the slice from 22°C to 32°C. Red traces are superimposed best fits to a single exponential at 22°C, 32°C and upon return of the temperature back to 22°C. The difference is undetectable. *Right*, blockade of Na^+/K^+–ATPase with bath–applied oubain (100 μM) had little effect on axonal Na^+ clearance. Red traces are superimposed best fits of decay of the Na^+ transients in control, during oubain application and following washout.

Figure 3 Axonal Na^+ transients reflect localized Na^+ influx into the AIS followed by diffusion to the soma and first myelinated internode.

(a) Experimentally observed (left) and simulated (right) changes in $[Na^+]_i$ elicited by a single AP.

(b) Similar $[Na^+]_i$ changes elicited by 10 APs at the indicated locations. The changes peaked after the end of the spike train (dashed line) at the dark blue and pink locations.

(c) The same $[Na^+]_i$ changes plotted as a function of distance from the soma for three different times after the last spike. Dots are average values (n=9).

(d) Times–to–peak of the Na^+ transients elicited by a single AP vs. distance from the axon hillock (n=5). Red continuous line calculated from a simplified model, assuming a 50 μm AIS.

(e) $[Na^+]_i$ changes elicited by 10 APs in pyramidal neurons and Purkinje neurons. *Left:* Times–to–peak of the Na^+ transients in pyramidal neurons (black, n=9) and in Purkinje neurons (blue,

n=5; see **Supplementary Fig. 1**) vs. distance from the soma. Continuous lines from the model, which assumed AIS length of 38 μm for pyramidal cells (red) and 15 μm for Purkinje cells (blue). *Right:* Impact of AIS length on width of the axonal Na^+ transients 10 μm from the hillock of pyramidal (black, n=8) and of Purkinje neurons (blue, n=5). Points are at the AIS lengths for the two cell types (15 μm for Purkinje cells and 40 μm for pyramidal cells). Red continuous line is the half–width of the simulated transients.

Figure 4 Shape of spike–evoked Na^+ transients constrains the ratio of Na^+ channel densities in different compartments.

(a) Na^+ transients elicited by ten (left) and one hundred (right) action potentials at the soma (black), in a basal dendrite (20 μm from the edge of the soma, blue) and in the AIS (20 μm from the hillock, red) of a representative neuron. Arrows indicate the points where the steady–state and the end–of–train fluorescence values were measured and the numbers are the ratios of the steady–state to end–of–train ΔF/F values.

(b) Na^+ transients in models with different process–to–soma ratios of Na^+ channel density. Somatic Na^+ channel density was kept constant and Na^+ channel density in the process was varied over the range of 0–30 times the somatic density (numbers along the left side of the figure). The numbers to the right of the traces are the calculated ratios of the steady–state to end–of–train signal. The model required the basal dendrite Na^+ channel density to be 0.1–0.3 times the somatic density and the AIS density to be 1–3 times the somatic density to match the experimentally determined signals.

Figure 5 Relative spike evoked Na^+ flux in different neuronal compartments.

(a) *Top:* ΔF/F and ΔF changes at the indicated locations (colored traces) elicited by a train of five action potentials. *Bottom:* pseudocolor maps of the changes between the times marked by the arrows.

(b) AP–evoked Na^+ charge transfer derived from the amplitude of Na^+ transients and morphological data. Dots represent individual measurements of $\frac{\Delta F \cdot volume}{F \cdot area}$ calculated for soma (n=14), AIS (n=14) and basal dendrites (n=9). Dashed lines are the mean values.

(c) AIS:soma and AIS:basal dendrite Na^+ charge transfer ratios calculated from ΔF (n=11) and $\frac{\Delta F \cdot volume}{F \cdot area}$ (n=9–14) values.

Figure 6 AP–evoked Na^+ charge transfer in nodes of Ranvier is comparable to the transfer in the AIS.

(a) *Left*, Reconstruction of a stack of 61 optical sections through part of a layer 5 pyramidal neuron filled with 2 mM SBFI. The first axonal branching point is ~100 μm from the hillock

(blue arrow). *Middle*, The same neuron as seen during the fluorescence imaging experiment with NeuroCCD–SMQ camera. *Right*, Averaged Na^+ transients (n=20) elicited by a train of five action potentials (200 Hz). See also **Supplementary Fig. 4**.

(b) Simulated changes in $[Na^+]_i$ elicited by a single AP plotted against distance from the axon hillock. The node was assumed to be 1 μm long and the AIS 45 μm. Dashed lines are $[Na^+]_i$ changes in a model with no Na^+ diffusion. Black continuous lines are $[Na^+]_i$ values 10 ms following the peak of the spike in the AIS and 0.7, 2 and 10 ms following the peak in the region around the node of Ranvier.

(c) Experimentally observed (left) and simulated (right) changes in $[Na^+]_i$ elicited by a train of five APs plotted against distance from the axon hillock. *Left*: Dots are averaged ΔF/F values from each 1.15 μm long pixel along the axon during the time interval 2–10 ms following the peak of the last spike in train. Red line – the AIS, blue arrow – the first node of Ranvier. *Right*, Changes in $[Na^+]_i$ in models with different node–to–AIS ratios of Na^+ channel density.

Figure 7 At subthreshold voltages, persistent Na^+ current is generated predominately in the AIS.

(a) 1 s, 70 pA current step to just subthreshold voltage, elicited a large $[Na^+]_i$ increase in the AIS (red trace). A brief (5 ms) pulse that generated a single AP caused a sharply rising Na^+ transient.

(b) Subthreshold pulses of 0.3, 1.0 and 3.0 s each generated a $[Na^+]_i$ increase that lasted the duration of the pulse. The rapid recovery at the end of the pulses shows that the current was active throughout. A sharply rising Na^+ transient elicited by a train of 5 action potentials at 50 Hz is shown for comparison.

(c) A just subthreshold, 1 s stimulus elicited a large $[Na^+]_i$ increase in the AIS (red trace) while the increase the soma (black trace) was much smaller. The train of 10 action potentials (40 Hz) caused sizable Na^+ transients in both locations.

(d) 2 s voltage ramp from –70 to –40 mV elicited Na^+ transients only in the axon. Interpolating along the ramp shows that I_{NaP} and axonal $[Na^+]_i$ both began to change at the same voltage (–57±6 mV; n=5).

(e) 2 s long voltage ramp from –70 to 0 mV elicited Na^+ signals which were clearly detectable in soma, basal and proximal apical dendrites. With this larger ramp the membrane current and AIS optical signals still began to change at –57±5 mV (n=21) but the signals in the soma and basal dendrites began to change at –41±5 mV (n=21).

Figure 8 Compartmental model of an AP that matches the fast maximal rates-of-rise of recorded spikes and initiates in the axon without requiring a high AIS Na^+ channel density.

(a) *Top, left*: blue: τ_m vs. V_m in a model based on published recordings[2]. Light blue and red: same relationships using scaling factors of 0.2 and 0.05. *Top, right*: single compartment

simulations of Na^+ currents produced by voltage steps from –100 mV to 0 mV as if recorded with an "open bandwidth" amplifier (continuous line) or filtered at 2 kHz. *Bottom, left*: axonal APs (left) and the first derivative of AP voltage (right) in the models with τ_m curves as indicated. The AIS Na^+ conductance was 500 pS/μm^2. *Bottom, right*: Maximal rate–of–rise vs. axonal Na^+ channel density (g_{Na}) if τ_m is 0 (black), using scaling factors of 0.05, 0.2 and 1 relative to the model[2]. Dashed line indicates 1130 V/s, the maximal measured rate–of–rise[3].

(b) Effect of AIS channel density and properties on AP initiation. *Top, left*: with AIS gNa as in the soma, the AP initiates simultaneously in the soma and in the AIS. *Top, right*: with 3X higher AIS gNa and with shifted voltage dependence, initiation shifted to the axon. *Bottom, left*: scaling Na^+ channel τ_m by 0.2 in all compartments increases the rate–of–rise, shifts the threshold and enhances the axo–somatic delays and voltage gradients. *Bottom, right*: with G_{NaP} 5% of the total AIS Na^+ conductance, the shifts in threshold and the axo–somatic delays and voltage gradients are greater.

Methods

Slice preparation and whole cell recording

Most experiments were performed on L5 pyramidal neurons from somatosensory neocortical coronal slices prepared from 2– to 4–week–old Sprague–Dawley rats [6, 35]. A few experiments were made from cerebellar Purkinje cells in sagittal slices from the same animals. Rats were anaesthetized with isoflurane and decapitated using procedures approved by the Institutional Animal Care and Use Committee of the Marine Biological Laboratory. Recordings were made from slices submerged in a plastic chamber with a glass bottom. The slices were superfused with warmed and oxygenated artificial cerebrospinal fluid (ACSF) at 32–34^{o}C except where noted. The composition of the ACSF was (in mM): 124 NaCl, 2.5 KCl, 2 $CaCl_2$, 2 $MgCl_2$, 1.25 NaH_2PO_4, 26 $NaHCO_3$, and 10 glucose; pH was 7.4 when bubbled with 95% O_2/CO_2.

The chamber with submerged and superfused slices was attached to a stage rigidly bolted to an air table and cells were viewed with a 20X, 40X or 60X water–immersion lens (Olympus, Melville, NY) in an Olympus BX50WI microscope mounted on an X–Y translation stage. Somatic whole–cell recordings were made using patch pipettes pulled from 1.5 mm outer diameter thick–walled borosilicate glass tubing (1511–M, Friderick and Dimmock, Millville, NJ). Tight seals were made with the "blow and seal" technique using video–enhanced DIC optics to visualize the cells[36]. For current clamp experiments the pipette solution contained (in mM): 140 K–gluconate, 4 NaCl, 4 Mg–ATP, 0.3 Na–GTP, and 10 HEPES, pH adjusted to 7.2–7.4 with KOH. This solution was supplemented with 2 mM SBFI and 2–4 μM Alexa–488 (Molecular Probes, Eugene, OR). The pipette solution for whole–cell voltage–clamp experiments contained (in mM): 135 CsCl, 4 NaCl, 2 $MgCl_2$, and 10 HEPES (cesium salt), pH 7.25, also supplemented with 2 mM SBFI and 2–4 μM Alexa–488; Ca^{2+} currents were blocked by adding 200 μM Cd^{2+} to the bath. For some experiments measuring dynamic $[Na^{+}]_i$ and $[Ca^{2+}]_i$ changes in the same cell, Alexa–488 was replaced with 50–100 μM of the high affinity Ca^{2+} indicator OGB–1 (Molecular Probes, Eugene, OR). Current clamp recordings were made with a Dagan BVC–700 amplifier; data were low–pass filtered at 10 kHz (–3dB, single–pole Bessel filter) and digitized at 20 kHz. Voltage clamp recordings were made with an Axopatch 200B amplifier; data were low pass filtered at 2 kHz (–3 dB, 4 pole Bessel filter) and sampled at 10 kHz. Care was taken to maintain membrane access resistance as low as possible (usually 3–4 MΩ and always less than 7 MΩ); series resistance was 80% compensated using the built–in circuitry of the amplifier.

Electrophysiological data analysis was accomplished using pCLAMP 10.0 (Axon Instruments) and Origin 6.0 (Origin Lab, Northampton, MA). If not otherwise noted, values are given as mean ± S.D. Student's *t*–test was used for statistical analysis.

Dynamic sodium and calcium measurements

SBFI fluorescence was excited with a 75W Xenon arc lamp using a Semrock (Rochester, NY) fura–2 filter set (EX=387(11) nm; DC=409 nm; EM=510(84) nm). For most experiments changes in fluorescence were acquired using a back–illuminated 80x80 pixel cooled CCD

camera (NeuroCCD–SMQ; RedShirt Imaging, Decatur, GA), controlled with Neuroplex software (RedShirtImaging). Images were acquired at 500 frames/s. Fluorescence changes from Purkinje cells (**Supplementary Fig. 1**) were detected with a Photometrics AT300 camera at 40 frames/s. To improve the signal to noise ratio of the traces 5–10 trials were typically averaged and the 500 Hz signals were smoothed with a five point moving average. Occasionally, more trials were averaged with no temporal filtering to improve the time resolution of the measurements. Signal averaging was limited by photodynamic damage to the preparation. To reduce this damage all positioning and focusing was done by monitoring the fluorescence from the co–injected Alexa–488 using an Olympus U–MWIBA filter set (EX=475(30) nm; DC=510 nm; EM=532(35) nm). In addition, the illumination intensity during sodium measurements sometimes was reduced with a 10X neutral density filter. Indicator bleaching was corrected by subtracting an equivalent trace without stimulation.

Fluorescence of the high affinity calcium indicator OGB–1was examined with the same U–MWIBA filter set using the same apparatus and camera. Images were acquired at 500 frames/s and responses were often averaged. Photodynamic damage was not a significant problem with this indicator. Data for both sodium and calcium measurements were analyzed using Neuroplex and SCAN, a custom software package written in our laboratory.

2–photon microscope reconstruction of cell morphology

At the end of many experiments we placed the slice that contained the cell(s) injected with SBFI in a beaker containing ACSF and carried it to a nearby Zeiss LSM–510 confocal microscope equipped with a Chameleon pulsed laser for 2–photon excitation. We first used a mercury arc lamp and a fura–2 filter set, similar to the one on our setup, to find the cell and place it in the center of the field using a 40X or 63X Zeiss water immersion lens. We then changed to 2–photon excitation at 740 nm and scanned the cell at 1.0 μm intervals. The resulting Z–stack was imported into NIH Image–J for reconstruction and image processing.

Sodium buffering

Intrinsic proteins and exogenous ion indicators can distort the amplitude and time course of ion concentration changes inside neurons and other cells. This is particularly true of measurements of $[Ca^{2+}]_i$ changes in pyramidal and other neurons. This buffering can be understood quantitatively by carefully measuring the amplitude and time course of the $[Ca^{2+}]_i$ change at different indicator concentrations and extrapolating to zero added indicator [37, 38]. In this formulation

$$\beta = \left(1 + \kappa_B + \kappa_{dye}\right)$$

is the buffering power, where κ_B and κ_{dye} are the ratios of the change in buffer bound Ca^{2+} to the change in free Ca^{2+} for a given Ca^{2+} influx for the cases where the buffer is an intrinsic protein (*B*) or an added indicator (*dye*). In a typical pyramidal neuron, when a low affinity Ca^{2+} indicator

is used, $\kappa_B \sim 100$ and $\kappa_{dye} \sim 10$. This means that $\beta \sim 111$ where $\beta = 1$ means no buffering. The peak $[Ca^{2+}]_i$ is reduced by factor β and the time constant for Ca^{2+} removal is increased by the same factor compared to the amplitude and rate in cells that have no Ca^{2+} buffers.

For $[Na^+]_i$ changes the same analysis applies but the effects of buffering are much different. First, there are almost no intrinsic Na^+ buffering molecules in the cytoplasm; the diffusion constant of Na^+ in cytoplasm (0.6 μm^2/ms) is almost the same value as in water [13, 39]. This means that $\kappa_B \sim 0$ for Na^+. Second, since the resting $[Na^+]_i$ (~4 mM) is much lower than the K_D for the SBFI:Na^+ reaction (~26 mM; reference [15]) then $\kappa_{dye} \sim [SBFI]/K_D$ (reference [37]). In our experiments typical [SBFI] was 2 mM. Therefore, $\kappa_{dye} \leq 0.1$. Combining the two values indicates that $\beta \sim 1.1$ for Na^+ in cytoplasm. Consequently, we expect little distortion of the true amplitude and time course of $[Na^+]_i$ changes by SBFI in our experiments.

Comparison of the Na^+ fluxes in different regions using ΔF

This approach (see text) has the advantage over $\Delta F/F$ measurement that it is not dependent on accurately measuring tissue autofluorescence. However, there are additional technical considerations, which we addressed as follows: If we want to determine the charge entry/unit membrane area then we must relate surface area to the area of a region measured in an imaging experiment (cross section). We simplify this comparison by assuming that the dendrites and axons are all cylinders and the soma is a sphere. Then there is no correction in comparing changes between dendritic regions and the axon. To compare the soma to the axon we have to correct by: $\frac{2\pi rl / 2rl}{4\pi r^2 / \pi r^2} = \pi/4 = 0.78$, which is the ratio of the surface of a cylinder to its cross section (what the camera images) divided by the same ratio for a sphere (r is the radius of the soma or the axon and l is the length of the axon segment).

When the axon or a dendrite is in focus, other elements may be slightly out of focus. Parts of the soma are inevitably out of focus since its thickness is significantly greater than the focal depth of the lens we use (usually 60X). To estimate whether these out of focus elements affect a quantitative estimate of the fluorescence intensity we measured the total fluorescence of 4 μm diameter fluorescent beads as we changed focus (**Supplementary Fig. 2a**).

We measured the fluorescence in a 10 μm diameter box surrounding the bead and found that the fluorescence changed by less than 10% with a change in focus of ±5 μm, even though the image clearly appeared out of focus. If the box was larger (~30 μm diameter) then the fluorescence did not change 10% for changes in focus of ±15 μm. Therefore, since the soma diameter is 22.9±4.3 μm (n=25; from 2–photon microscope reconstructions) it is likely that the error in measuring the cell fluorescence is <10% if a measuring box is chosen appropriately. If there is an error in estimating the signal size from the soma it is likely to be an underestimate since the signals from out of focus elements are smaller. In a related series of experiments we

also determined that the combined sensitivity of the camera and the evenness of the fluorescence excitation over the field of view did not vary by more than 5%.

We tried to minimize the effects of diffusion on these measurements by using short trains of 5 spikes at 100 Hz to generate the $[Na^+]_i$ increase. In this case the rising phase of the signal is much faster than the decay rate and there is little effect of diffusion on the peak amplitude except at locations very close to the soma (see **Figs 1 and 3**). In other experiments we measured the fluorescence signals from trains of 10 APs evoked at 30 ms intervals in order to improve the S/N of the measurements. In this case the removal rate in the axon is comparable to the influx rate and the amplitude of the fluorescence change is not proportional to the total Na^+ entry. In the soma and dendrites the removal rate is much slower and the peak amplitude should be proportional to Na^+ entry.

To correct for the distortion in the peak amplitude due to the rapid removal of Na^+ in the axon we constructed a simple model of Na^+ entry in the AIS and soma and removal by diffusion and compared the peak fluorescence change in the case of normal Na^+ diffusion (which accurately replicates the $[Na^+]_i$ changes in these regions; **Fig. 3**), with the results of a model where the diffusion constant was set to zero. The latter case corresponds to the situation with no removal, so the peak amplitude should be proportional to Na^+ entry. The model showed that in the center of the AIS the peak amplitude with normal diffusion is about 70% of the amplitude without diffusion in the case where 10 APs are generated at 30 ms intervals (total stimulation time of 300 ms); closer to the ends of the AIS the differences are greater because Na^+ in those regions is rapidly diffusing into the soma or the myelinated region of the axon. As expected, the difference is much less for a short train of 50 ms (except next to the soma) and greater for a longer train. These differences are substantial for the longer trains and are the largest corrections that must be applied to estimate the true relative Na^+ entry in different regions during a slower spike train.

Modeling Na^+ diffusion and electrophysiological properties

Numerical simulations were performed in the NEURON simulation environment [40]. Unless otherwise stated, electrophysiological parameters and dynamic $[Na^+]_i$ changes were studied in a simplified compartmental model that encompassed the fundamental morphological and electrical features of Layer 5 pyramidal and Purkinje neurons. In the model the 1.2 –2 μm thick AIS extended over the first 40–50 μm of the axon in L5 pyramidal cells and 15 μm in Purkinje cells. The subsequent segment (length: 50 μm; diameter 1.2 μm) was myelinated. The first node of Ranvier (length: 1 μm; diameter 1.2 μm) was positioned at 100 μm from the soma, which approximately corresponded with the location of the experimentally observed localized $[Na^+]_i$ increases (see **Fig. 8**). The soma (length: 35 μm; diameter: 23 μm) gave rise to a single apical dendrite (length: 700 μm; diameter: 3.5 μm) and to two basal dendrites (length: 200 μm; diameter: 1.2 μm). For computational precision all compartments were divided into many segments with the length of individual segments usually less than 1 μm. The passive electrical

properties R_m, C_m and R_i were set to 15,000 Ω cm^2, 0.9 μF cm^{-2} and 125 Ω cm, respectively, uniformly throughout all compartments. Myelination was simulated by reducing C_m to 0.02 μF cm^{-2}. The resting membrane potential at the soma was set to –75 mV. All simulations were run with 5 μs time steps and the nominal temperature of simulations was 32°C.

The model incorporated a Hodgkin–Huxley based Na^+ conductance as previously described[2]. The activation time constant was given by $\tau_m = k/(\alpha_m(V_m) + \beta_m(V_m))$; unless otherwise stated, the scaling factor, *k,* was 0.2 (see **Fig. 8a**). The Na^+ conductance was 250 pS μm^{-2} in the soma, 200 pS μm^{-2} in the apical dendrite, 40 pS μm^{-2} in the basal dendrites, 750 pS μm^{-2} in the AIS, and 1200 pS μm^{-2} in the nodes of Ranvier. Myelinated internodes possessed no Na^+ channels. These densities were tuned to account for previously published AP characteristics [1, 19, 26, 41] and for the measured Na^+ fluxes in the different neuronal compartments. Thus, the somatic Na^+ conductance was set to 250 pS μm^{-2} (maximal m^3h of ~220 pS μm^{-2}) in order to achieve a maximal spike upstroke velocity of ~500 V/s and Q_{Na} of ~12 fC/μm^2. This value is consistent with the channel density as calculated from the data on isolated cortical pyramidal neurons[22]. In the model, persistent Na^+ conductance differed from the transient Na^+ conductance in that there was no inactivation variable and voltage dependence of activation that was shifted to the left by 10 mV. The model included Kv and Kv1–like K^+ channels with kinetics and density as previously described[3]. The K^+ equilibrium potential was set to –85 mV.

Diffusion of Na^+ was modeled as the exchange of Na^+ ions between adjacent neuronal compartments using the intrinsic protocols in NEURON assuming a diffusion coefficient of 0.6 μm^2/ms (reference 13). The resting intracellular and the extracellular Na^+ concentrations were set to 4 and 151 mmol/l, respectively.

References

1. Kole, M.H. & Stuart, G.J. Is action potential threshold lowest in the axon? *Nat. Neurosci.* **11**, 1253–1255 (2008).
2. Colbert, C.M. & Pan, E. Ion channel properties underlying axonal action potential initiation in pyramidal neurons. *Nat. Neurosci.* **5**, 533–538. (2002).
3. Kole, M.H.*, et al.* Action potential generation requires a high sodium channel density in the axon initial segment. *Nat. Neurosci.* **11**, 178–186 (2008).
4. Hu, W.*, et al.* Distinct contributions of Na(v)1.6 and Na(v)1.2 in action potential initiation and backpropagation. *Nat. Neurosci.* **12**, 996–1002 (2009).
5. Stuart, G. & Sakmann, B. Amplification of EPSPs by axosomatic sodium channels in neocortical pyramidal neurons. *Neuron* **15**, 1065–1076. (1995).
6. Astman, N., Gutnick, M.J. & Fleidervish, I.A. Persistent sodium current in layer 5 neocortical neurons is primarily generated in the proximal axon. *J. Neurosci.* **26**, 3465–3473 (2006).
7. Mainen, Z.F., Joerges, J., Huguenard, J.R. & Sejnowski, T.J. A model of spike initiation in neocortical pyramidal neurons. *Neuron* **15**, 1427–1439 (1995).
8. Colbert, C.M. & Johnston, D. Axonal action–potential initiation and Na+ channel densities in the soma and axon initial segment of subicular pyramidal neurons. *J. Neurosci.* **16**, 6676–6686. (1996).
9. Minta, A. & Tsien, R.Y. Fluorescent indicators for cytosolic sodium. *J. Biol. Chem.* **264**, 19449–19457 (1989).
10. Callaway, J.C. & Ross, W.N. Spatial distribution of synaptically activated sodium concentration changes in cerebellar Purkinje neurons. *J. Neurophysiol.* **77**, 145–152. (1997).
11. Palmer, L.M. & Stuart, G.J. Site of action potential initiation in layer 5 pyramidal neurons. *J. Neurosci.* **26**, 1854–1863 (2006).
12. Lelievre, L., Zachowski, A., Charlemagne, D., Laget, P. & Paraf, A. Inhibition of (Na+ + K+)–ATPase by ouabain: involvement of calcium and membrane proteins. *Biochim. Biophys. Acta* **557**, 399–408 (1979).
13. Kushmerick, M.J. & Podolsky, R.J. Ionic mobility in muscle cells. *Science* **166**, 1297–1298 (1969).
14. Clark, B.A., Monsivais, P., Branco, T., London, M. & Hausser, M. The site of action potential initiation in cerebellar Purkinje neurons. *Nat. Neurosci.* **8**, 137–139 (2005).
15. Rose, C.R., Kovalchuk, Y., Eilers, J. & Konnerth, A. Two–photon Na+ imaging in spines and fine dendrites of central neurons. *Pflugers Arch.* **439**, 201–207. (1999).
16. Peters, A. The node of Ranvier in the central nervous system. *Q. J. Exp. Physiol. Cogn. Med. Sci.* **51**, 229–236 (1966).
17. Fleidervish, I.A. & Gutnick, M.J. Kinetics of slow inactivation of persistent sodium current in layer V neurons of mouse neocortical slices. *J. Neurophysiol.* **76**, 2125–2130. (1996).
18. Alzheimer, C., Schwindt, P.C. & Crill, W.E. Modal gating of Na+ channels as a mechanism of persistent Na+ current in pyramidal neurons from rat and cat sensorimotor cortex. *J. Neurosci.* **13**, 660–673 (1993).

19. Kole, M.H., Letzkus, J.J. & Stuart, G.J. Axon initial segment Kv1 channels control axonal action potential waveform and synaptic efficacy. *Neuron* **55**, 633–647 (2007).
20. Engel, D. & Jonas, P. Presynaptic action potential amplification by voltage–gated Na+ channels in hippocampal mossy fiber boutons. *Neuron* **45**, 405–417 (2005).
21. Royeck, M.*, et al.* Role of axonal NaV1.6 sodium channels in action potential initiation of CA1 pyramidal neurons. *J. Neurophysiol.* **100**, 2361–2380 (2008).
22. Carter, B.C. & Bean, B.P. Sodium entry during action potentials of mammalian neurons: incomplete inactivation and reduced metabolic efficiency in fast–spiking neurons. *Neuron* **64**, 898–909 (2009).
23. Bender, K.J. & Trussell, L.O. Axon initial segment Ca2+ channels influence action potential generation and timing. *Neuron* **61**, 259–271 (2009).
24. Lasser–Ross, N. & Ross, W.N. Imaging voltage and synaptically activated sodium transients in cerebellar Purkinje cells. *Proc. R. Soc. Lond. B. Biol. Sci.* **247**, 35–39. (1992).
25. Alle, H., Roth, A. & Geiger, J.R. Energy–efficient action potentials in hippocampal mossy fibers. *Science* **325**, 1405–1408 (2009).
26. Nevian, T., Larkum, M.E., Polsky, A. & Schiller, J. Properties of basal dendrites of layer 5 pyramidal neurons: a direct patch–clamp recording study. *Nat. Neurosci.* **10**, 206–214 (2007).
27. Acker, C.D. & Antic, S.D. Quantitative assessment of the distributions of membrane conductances involved in action potential backpropagation along basal dendrites. *J. Neurophysiol.* **101**, 1524–1541 (2009).
28. Bean, B.P. The action potential in mammalian central neurons. *Nat. Rev. Neurosci.* **8**, 451–465 (2007).
29. Sugihara, I., Lang, E.J. & Llinas, R. Uniform olivocerebellar conduction time underlies Purkinje cell complex spike synchronicity in the rat cerebellum. *J. Physiol.* **470**, 243–271 (1993).
30. Markram, H., Lubke, J., Frotscher, M. & Sakmann, B. Regulation of synaptic efficacy by coincidence of postsynaptic APs and EPSPs. *Science* **275**, 213–215 (1997).
31. Shrager, P. The distribution of sodium and potassium channels in single demyelinated axons of the frog. *J. Physiol.* **392**, 587–602 (1987).
32. Zhang, C.L., Wilson, J.A., Williams, J. & Chiu, S.Y. Action potentials induce uniform calcium influx in mammalian myelinated optic nerves. *J. Neurophysiol.* **96**, 695–709 (2006).
33. Attwell, D. & Iadecola, C. The neural basis of functional brain imaging signals. *Trends in Neurosciences* **25**, 621 (2002).
34. Mata, M., Fink, D.J., Ernst, S.A. & Siegel, G.J. Immunocytochemical demonstration of Na+,K(+)–ATPase in internodal axolemma of myelinated fibers of rat sciatic and optic nerves. *J. Neurochem.* **57**, 184–192 (1991).
35. Larkum, M.E., Watanabe, S., Nakamura, T., Lasser–Ross, N. & Ross, W.N. Synaptically activated Ca2+ waves in layer 2/3 and layer 5 rat neocortical pyramidal neurons. *J. Physiol.* **549**, 471–488 (2003).

36. Stuart, G.J., Dodt, H.U. & Sakmann, B. Patch–clamp recordings from the soma and dendrites of neurons in brain slices using infrared video microscopy. *Pflugers Arch.* **423**, 511–518. (1993).
37. Helmchen, F., Imoto, K. & Sakmann, B. Ca2+ buffering and action potential–evoked Ca2+ signaling in dendrites of pyramidal neurons. *Biophys. J.* **70**, 1069–1081 (1996).
38. Neher, E. & Augustine, G.J. Calcium gradients and buffers in bovine chromaffin cells. *J. Physiol.* **450**, 273–301 (1992).
39. Hodgkin, A.L. & Keynes, R.D. Experiments on the injection of substances into squid giant axons by means of a microsyringe. *J. Physiol.* **131**, 592–616 (1956).
40. Hines, M.L. & Carnevale, N.T. The NEURON simulation environment. *Neural Comput.* **9**, 1179–1209 (1997).
41. Stuart, G., Schiller, J. & Sakmann, B. Action potential initiation and propagation in rat neocortical pyramidal neurons. *J. Physiol.* **505**, 617–632. (1997).

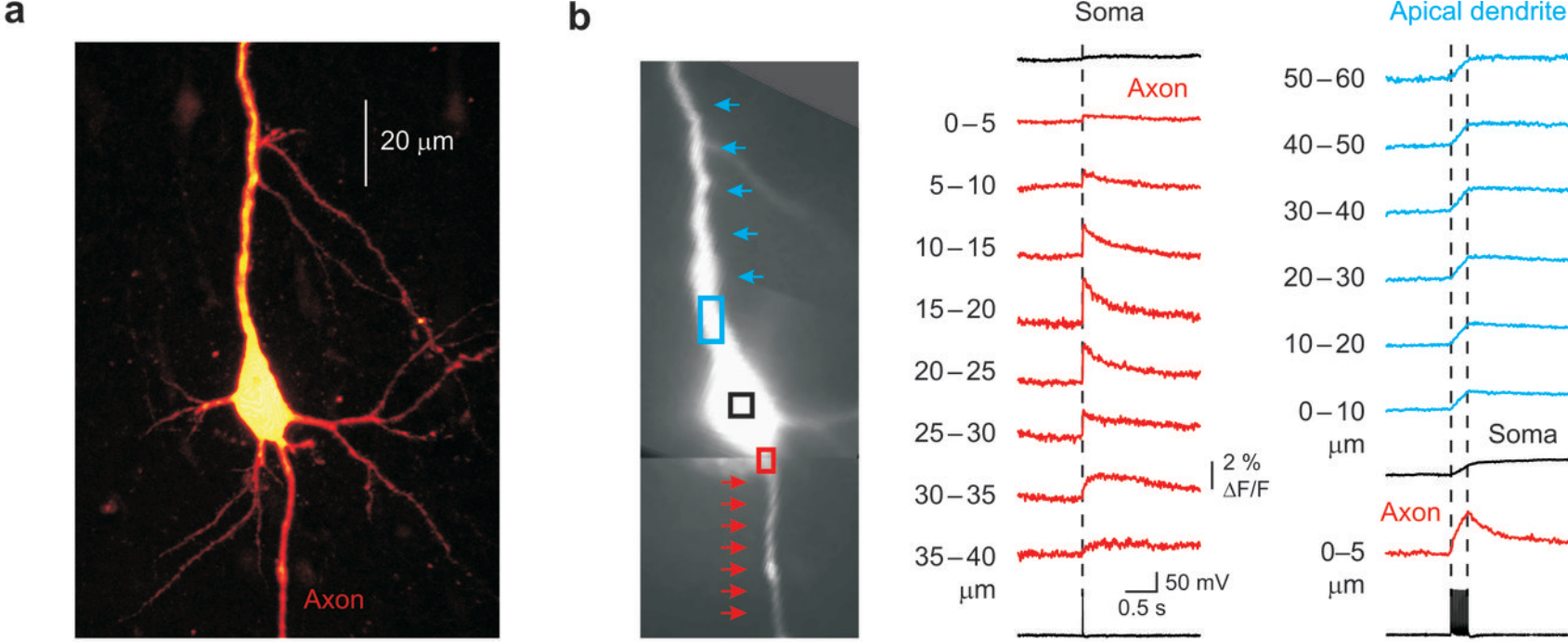

Figure 1 Fleidervish et al.

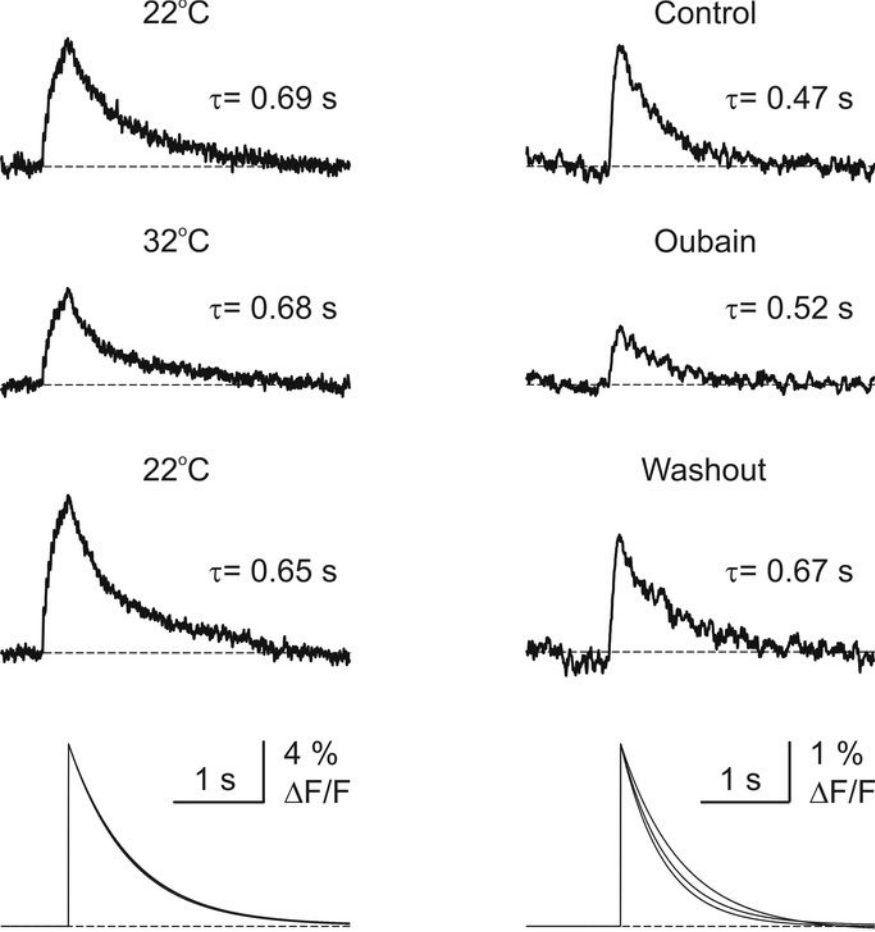

Figure 2 Fleidervish et al.

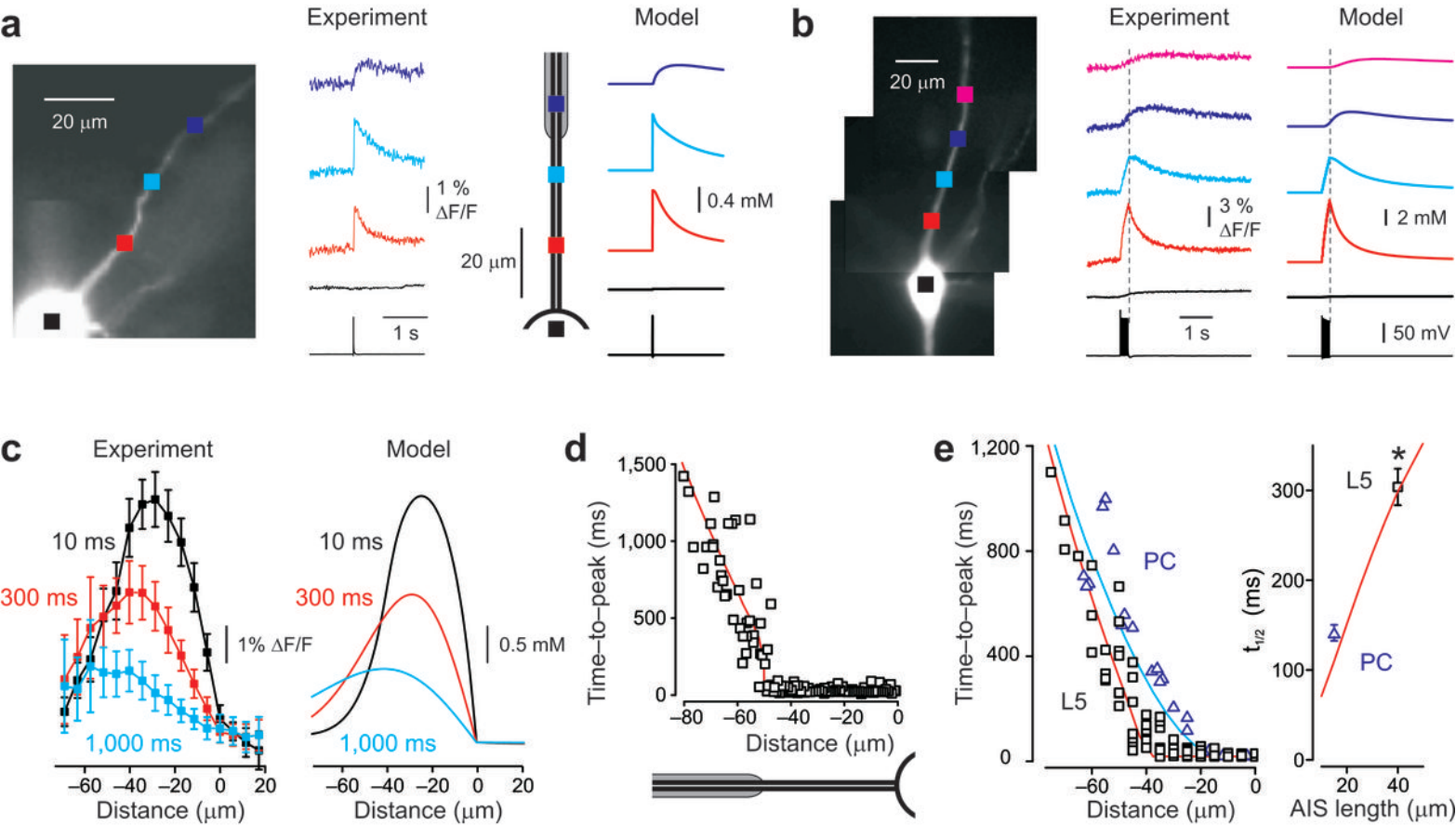

Figure 3 Fleidervish et al.

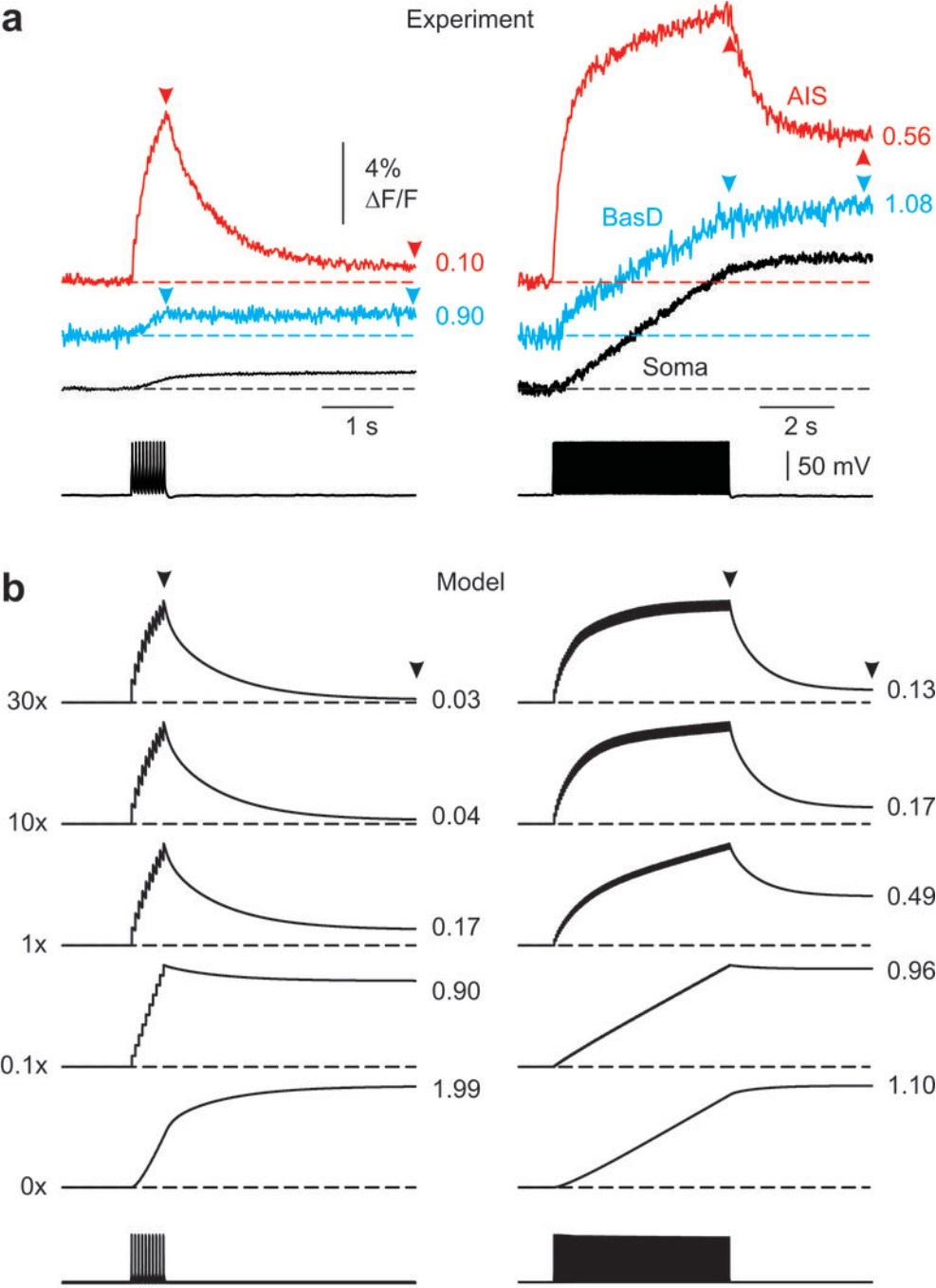

Figure 4 Fleidervish et al.

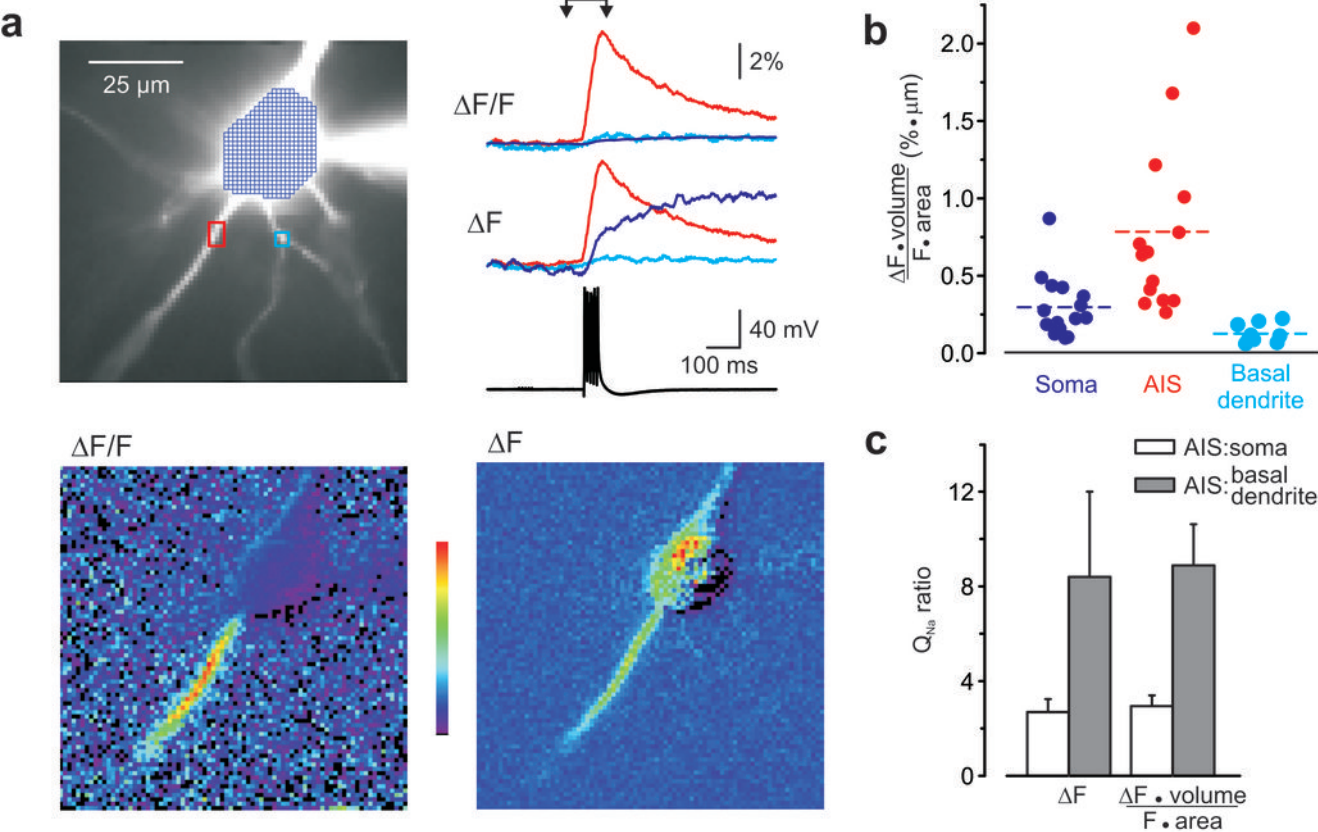

Figure 5 Fleidervish et al.

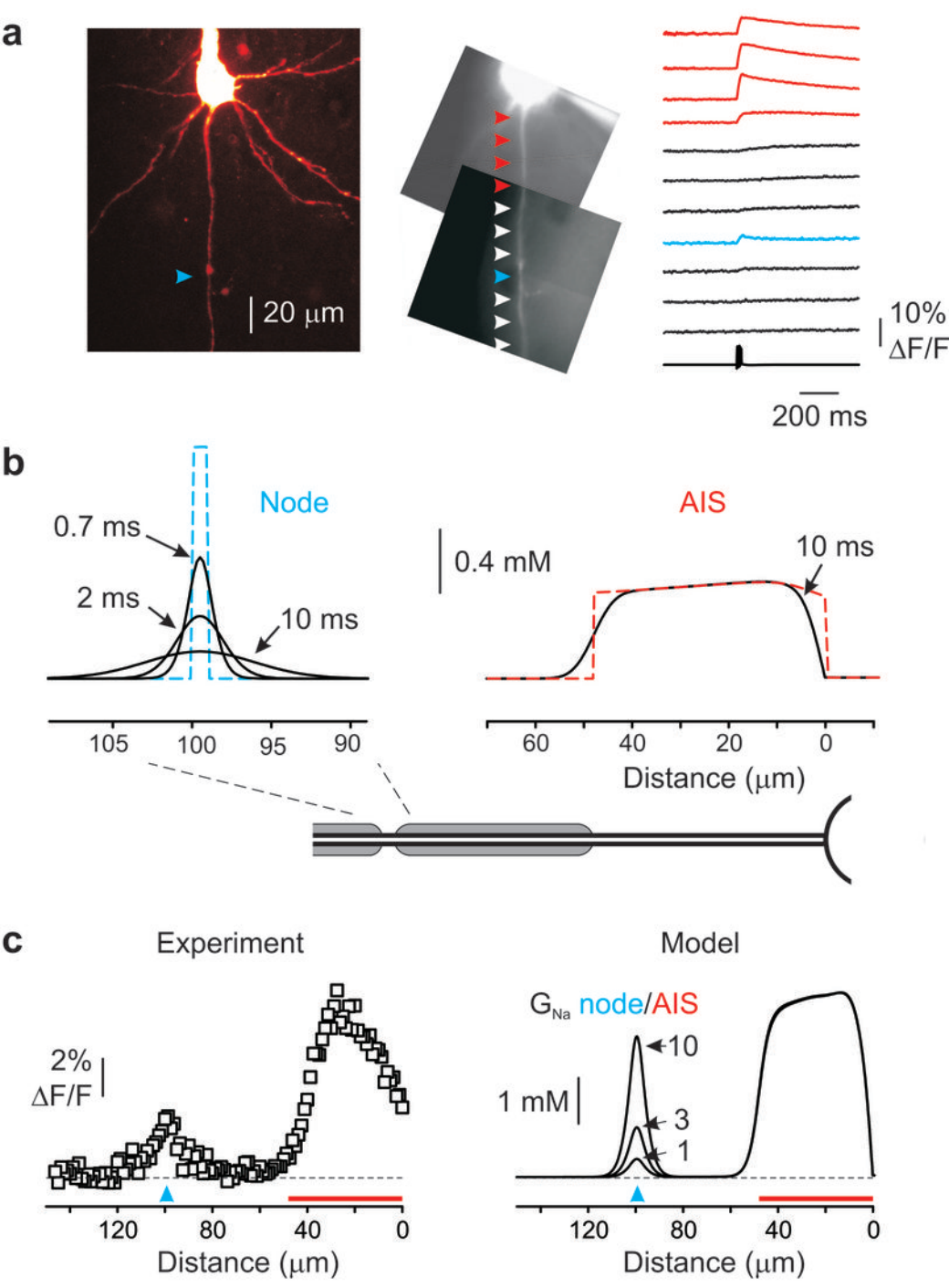

Figure 6 Fleidervish et al.

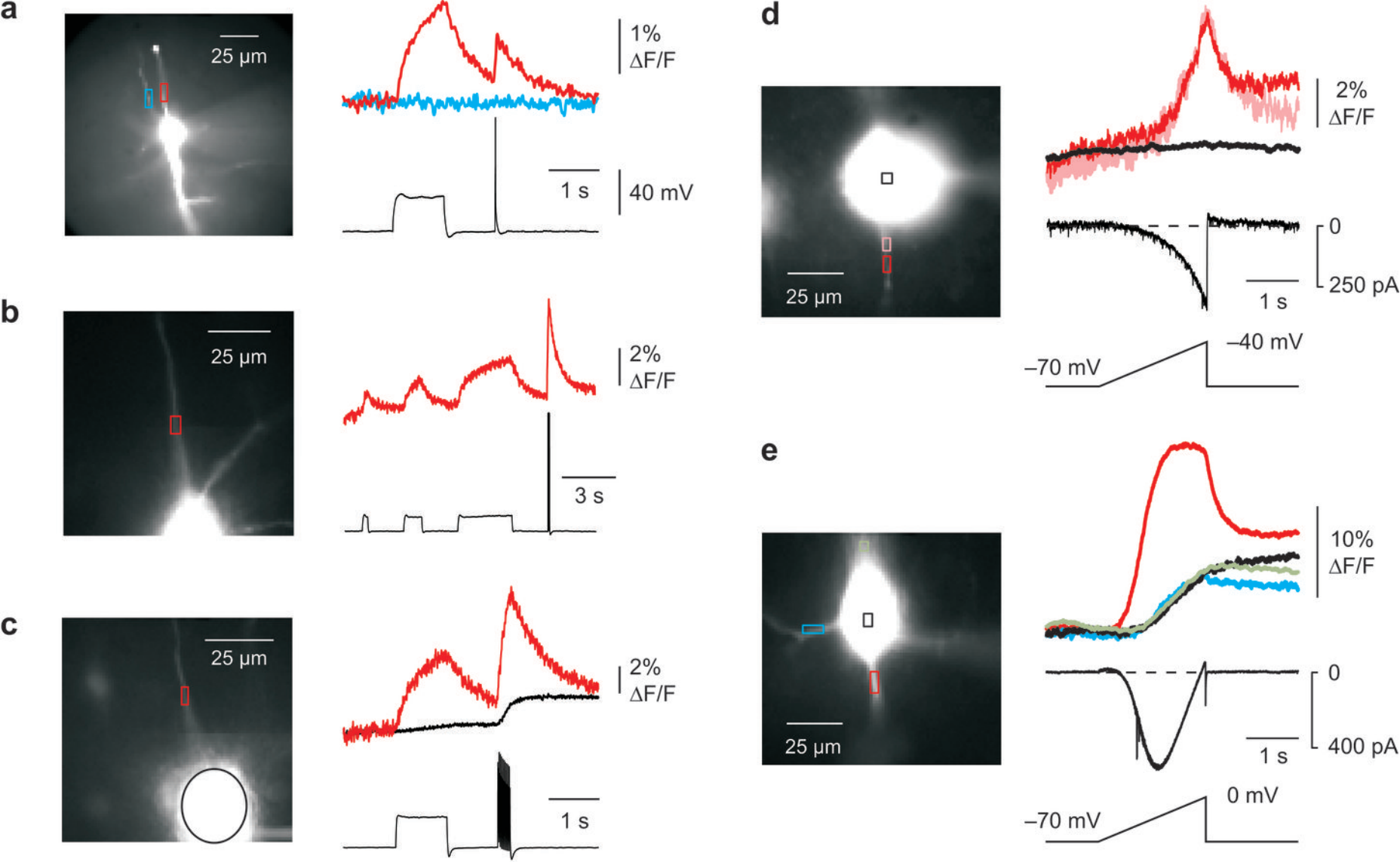

Figure 7 Fleidervish et al.

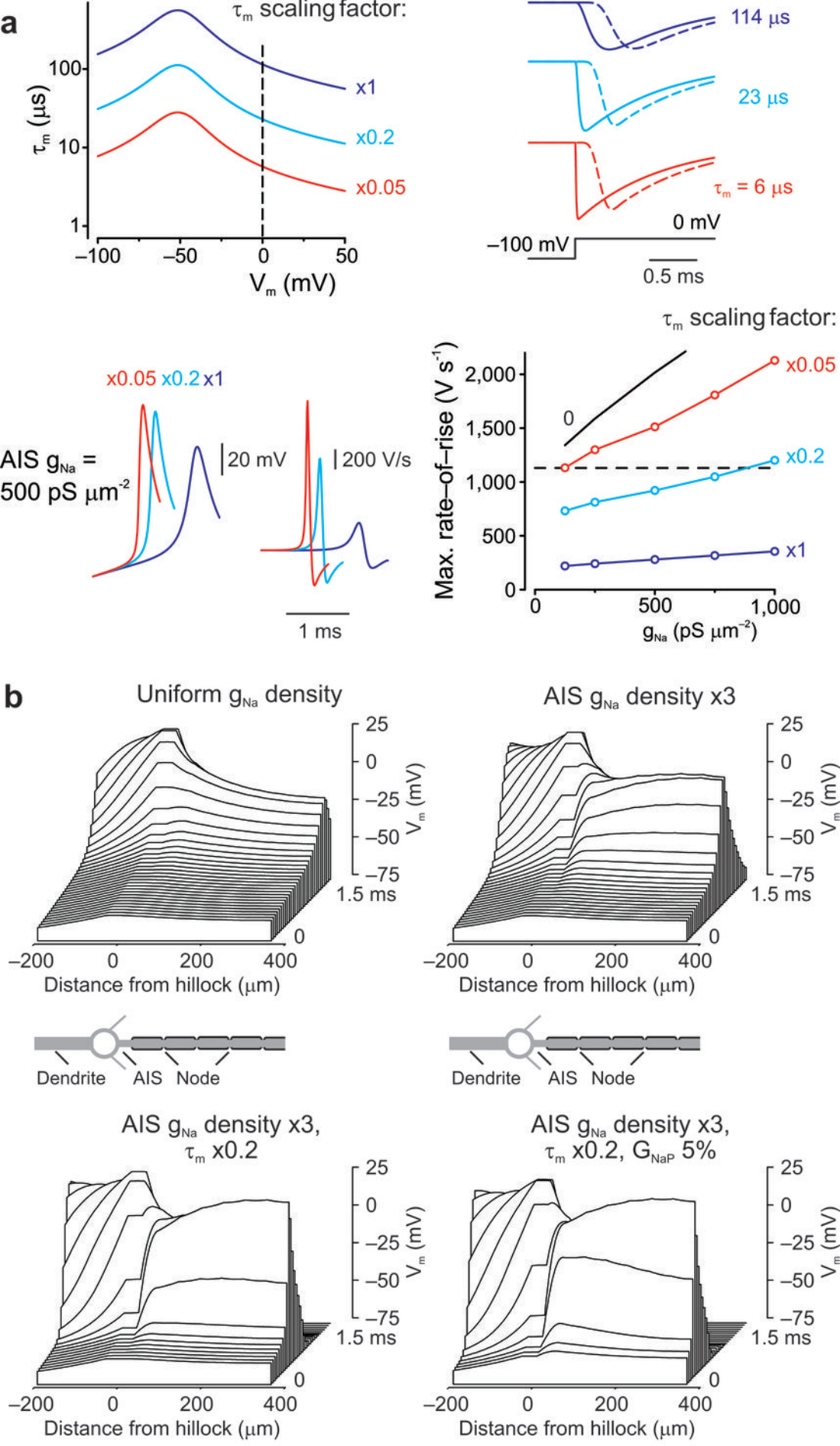

Figure 8 Fleidervish et al.